

# Chapter 10. Radiation Shielding and Activation

O. E. Krivosheev and N. V. Mokhov

## 10.1. Introduction

Radiation transport analysis, which includes accelerator and nuclear physics, shielding, activation, engineering, and safety analyses, is critical to almost all operations important to the design and construction of an intense high-energy accelerator facility like the proposed Proton Driver. As in similar projects of this type, such as the Spallation Neutron Source, these analyses are fundamentally important because of the impact on machine performance, conventional facility design, maintenance operations, and because the costs associated with incorporating the results of the radiation transport analysis can comprise a significant part of the total facility costs [1].

A very high beam power implies serious constraint on beam losses in the machine [2]. Only with a very efficient beam collimation system [3] can one reduce uncontrolled beam losses in the machine to an allowable level (see Chapter 9). The design strategy of the Proton Driver is that the beam losses are localized and controlled as much as possible via the dedicated beam collimation system described in Chapter 9. This way, the source term for the radiation analysis is a derivative of the collimation system performance with a high loss rate localized in the injection/collimation section and drastically lower uncontrolled beam loss rate in the rest of the lattice. As will be shown below, the main concerns are hands-on maintenance and ground-water activation. Massive local shielding is needed around the collimators. The entire complex must be well shielded to allow a non-controlled access to the outside surfaces under normal operation and accidental beam loss.

The radiation transport analysis of the Proton Driver can be subdivided into two major categories: (1) *Prompt radiation* and (2) *Residual radiation*. The first drives shielding design and analysis to meet direct radiation criteria for non-controlled areas. It also determines beam-induced energy deposition effects in equipment: instantaneous and steady-state temperature rise, dynamic heat load to the cooling systems, dose accumulated in the machine components that causes material damage and limits component lifetime. The second category includes radio-activation of equipment (hands-on maintenance), ground and ground water, and air.

Thorough Monte Carlo calculations were performed for realistic assumptions and geometry under normal operation and accidental conditions. This allowed one to deduce the tolerable beam losses (see Chapter 9) and conduct shielding design and analysis in all aspects which impact on machine performance, conventional facility design and maintenance operations. Several issues—such as air and dirt activation—are left aside, because of the absence of corresponding input information at this stage and as it was estimated they are not critical factors in shielding design and analysis.

## 10.2. Regulatory Requirements

1. *Prompt radiation*: the criterion for dose rate in non-controlled areas on accessible outside surfaces of the shield is 0.05 mrem/hr at normal operation and 1 mrem/hr for the worst case due to accidents [4]. Currently, the Fermilab Radiological Control Manual (FRCM) [4] uses the phrase “credible accident”. The ability to tolerate a one hour continuous maximum intensity loss was required in the past, but is no longer required under all conditions. In many cases, it is not even possible for a machine to do this. The FRCM [4] requires that the machine designers describe and justify what a possible credible worst case accident is, and design the shielding—or modify operation of the machine—accordingly [5].
2. *Hands-on maintenance*: residual dose rate of 100 mrem/hr at 30 cm from the component surface, after 100 day irradiation at 4 hrs after shutdown. Averaged over the components, the dose rate should be less than 10-20 mrem/hr. It is worth noting that the (100 days / 4 hrs / 30 cm) condition is practically equivalent to the (30 days / 1 day / 0 cm) one.
3. *Ground-water activation*: do not exceed radionuclide concentration limits  $C_{i,reg}$  of 20 pCi/ml for  $^3\text{H}$  and 0.4 pCi/ml for  $^{22}\text{Na}$  in any nearby drinking water supplies. These limits mean that if water containing only one of the radionuclides at the limit was used by someone as their primary source of drinking water, that individual would receive an annual dose equivalent of 4 mrem.

Additionally, we assume the accumulated dose of 20 Mrad/yr or 400 Mrad over 20 years lifetime in the hot spots of machine components as a *radiation damage* limit for such materials as epoxy and cable insulation.

## 10.3. Ground-Water Activation

Ref. [4] defines the concentration limits for the two long-lived isotopes that most easily leach and migrate to the ground water:  $^3\text{H}$  (half-life time  $\tau_{1/2}=12.32$  yr,  $\beta^-$  decay mode) and  $^{22}\text{Na}$  ( $\tau_{1/2}=2.604$  yr,  $\beta^+$  and  $\gamma$  decay modes). One needs to calculate creation and build-up of those nuclides. After irradiation over the time  $t$ , the concentration of a radionuclide  $i$  in the ground water in soil immediately outside the beam loss region is

$$C_i\left(\frac{\text{pCi}}{\text{ml}}\right) = \frac{1}{0.037} N_p S_{av} \frac{K_i L_i (1 - e^{-t/\tau_i})}{n}, \quad (10.1)$$

where  $N_p$  is the number of protons per second at the source,  $S_{av}$  is the star density above 50 MeV (stars/cm<sup>3</sup>/proton) averaged over a volume surrounding the source out to an appropriate boundary (e. g., to 0.1% of the maximum star density at the entrance to the soil, that is a “99.9% star volume”),  $K_i$  is the radionuclide production yield (atoms/star),  $L_i$  is the leachability factor,  $n$  is the soil porosity, and  $\tau_i$  is the mean lifetime of the radionuclide  $i$ ,  $\tau_i = \tau_{1/2} / \ln 2$ . The soil porosity  $n$  is the ratio of the volume of void in the soil (generally filled with water), to the volume of rock (unitless).  $n = \rho w_i$ , where  $w_i$  is the mass

of water per unit mass of soil that corresponds to the leaching fraction of the  $i$ th nuclide and  $\rho$  is the soil density.  $K_i L_i$  and  $w_i$  are site specific parameters. For example,  $K_{3H} L_{3H} = 0.075$  atoms/star,  $K_{22Na} L_{22Na} = 0.0035$  atoms/star and  $n=0.30$  for the glacial till of the Fermilab NuMI project [6].

The sum of the fractions of radionuclide contamination (relative to regulatory limits  $C_{i,reg}$ ) must be less than one for all radionuclides [6, 7]:

$$C_{tot} = \sum_{i=1}^N \frac{R_i C_i}{C_{i,reg}} \leq 1, \quad (10.2)$$

where  $R_i$  is the reduction factor for the nuclide  $i$  due to vertical transport through the material surrounding the tunnel and horizontal transport in the aquifer. Usually,  $R_i$  is taken to be unity in such materials as dolomite, but  $R_i < 1$  in glacial till and similar materials [7]. Using  $R_i=1$  would therefore overestimate the result [5].

It is useful to know a MARS calculated hadron flux  $\Phi_h^0$  above a given threshold immediately outside the tunnel wall, which corresponds to  $C_{tot}=1$ . For the NuMI case, with a 120 GeV proton beam on a thin 1-m long graphite target in the center of a 2-m radius tunnel with 40-cm thick concrete walls,  $\Phi_h^0(E > 30 \text{ MeV})=3640 \text{ cm}^{-2}\text{s}^{-1}$ . That is rather close to  $\Phi_h^0(E > 30 \text{ MeV})=4000 \text{ cm}^{-2}\text{s}^{-1}$  used in reference [6]. For the 16-GeV Proton Driver arcs, this flux outside a 40-cm thick concrete wall which is 1.6 m from a beam axis, is  $\Phi_h^0(E > 30 \text{ MeV})=3450 \text{ cm}^{-2}\text{s}^{-1}$  and  $\Phi_h^0(E > 20 \text{ MeV})=3850 \text{ cm}^{-2}\text{s}^{-1}$ . The fraction of  $^3H$  contamination is about 30%, while that of  $^{22}Na$  is about 70%.

## 10.4. Radiation Analysis Methodology

### 10.4.1. Normal operation and beam accident

The shielding analysis for the beam transport lines, arcs and long straight sections is performed both for normal operation and for accidental beam loss. The simplest operational scenario is a 1 W/m beam loss rate distributed uniformly along the beam line. A realistic one is based on the beam loss distributions of Chapter 9 with the average rates in the arcs of about 0.2 W/m at the top energy and less than 0.05 W/m at injection. In all cases, beam loss and local shielding (see below) in the collimation region are determined from realistic distributions in the P20 straight section calculated in this study. With the long bare drifts in the arcs and P20 section components locally shielded to meet hands-on maintenance limits, the ground-water protection requirements (see Chapter 9) are fulfilled. Certainly, the 4 MW Phase II of this project would require further consideration of radiation shielding issues. Prevention of ground-water flow in a vicinity of the tunnel wall is an additional possibility here. The shielding against prompt radiation is designed such that the dose rate on accessible outer surfaces of the shield is less than 0.05 mrem/hr in non-controlled areas.

For the worst case catastrophic *incredible* accident we assume a loss of the full 1.2 MW of beam at a single point, with the shielding reducing the dose on accessible outside surfaces of the shield to less than 1 mrem/hr in non-controlled areas. The new DOE regulations now

allow for credit to be taken for active shutdown measures, allowing one to address *credible* beam spill accidents with respect to the shield design [8]. In the current Proton Driver design, the “worst credible accident” approach is used, which would limit the amount of beam lost in such an accident to about 0.1% of that in the *incredible* case.

#### 10.4.2. MARS modeling

The MARS code system [9] is used to perform all the calculations in this study. A new interface library has been developed—using ideas and the code of Ref. [10]—which allows one to read and build a complex machine geometry directly from the MAD lattice description. The call-back mechanism is used to achieve such a goal. The user describes the geometry components at  $\vec{r} = \vec{0}$  and unrotated, their field, materials and volumes as callable functions with well-defined signature and registers them with the MAD interface code. Using information on the lattice description, MAD generates rotation matrices and translation vectors for the particular element together with glue elements. The call-back mechanism also allows one to register and call specific geometry, field and initialization function for any non-standard element in the lattice. The dipole, quadrupole and sextupole field components from the MAD lattice description are transferred to the respective field functions in order to correlate the field with lattice bending angle. An example of the lattice model geometry generated is shown in Fig. 9.3. Using this MAD/MARS interface, the arc cells were built for the 16 GeV Proton Driver lattice. The beam lines include magnets, quadrupoles, bare beam pipes (drifts) and tunnel geometry. The magnetic fields for the particular components were also implemented in the model. Typical cross-section views of the lattice elements in the calculation model are shown in Fig. 9.4.

To estimate tolerable beam loss, it is assumed that the beam loss rate is quasi-uniform along the arc region considered and that protons hit the beam-pipe under a grazing angle of 1 mrad horizontally inwards (see Chapter 9). The results are normalized to a beam loss of 1 W/m, which is equivalent to  $3.9 \times 10^8$  protons/m/s for a 16 GeV machine.

In MARS calculations for shielding and activation analysis, more realistic beam loss distributions from Chapter 9 have been used as generated with a tracking code STRUCT [11]. Calculated are energy deposition in dipole and quadrupole coils, residual dose rates on contact to the lattice elements and shielding, and dose and particle flux distributions in the tunnel cross-section. The latter are averaged over the “99.9% volume” star density in soil to calculate the ground-water activation assuming a 20 yr irradiation time and the glacial till parameters with  $R_i=1$ , and dose distribution in soil to estimate shielding parameters.

#### 10.4.3. Benchmarking and uncertainties

Reliable calculation of dose attenuation in the shielding to allowable levels is a non-trivial problem. Several techniques—such as biasing, mathematical expectation, exponential transformation and a combination of Monte Carlo with deterministic methods—are used to reach probability levels of  $\sim 10^{-10}$ . The uncertainties of the radiation field predictions over such a dynamic range are not easy to quantify. The most direct way is benchmarking against experimental data and other reliable simulation codes.

There has been substantial progress with Monte-Carlo code developments and validation over the last several years. The current versions of the MARS [9], FLUKA [12, 13] and MCNPX [14] codes are obvious leaders. These days, if an expert uses the right code, energy deposition, particle fluxes and related values can be predicted with a 10% accuracy in a majority of cases. Residual dose rate calculation uncertainty is within a factor of two.

Recently, two code verifications have been performed with independent calculation methodologies. The first was for a simplified model of the SNS Linac tunnel [15]. A section of the tunnel was modeled as a cylindrical shell of concrete 2.3 m in radius, 0.46 m thick and 30 m long. The tunnel was filled with air and surrounded by 9 m of earth berm for shielding. A 0.15 m diameter by 1 m cylinder of copper in the center of the geometry simulated the interaction of the 1 GeV proton beam with accelerator components. The ORNL, BNL and FNAL teams provided their results for this benchmarking. Fig. 10.1 shows dose attenuation in the earth berm predicted in six different approaches. The FNAL results obtained with the MARS code [9] closely match the ORNL ones obtained with the most recent version of the LANL MCNPX-CEM code [14] and are within a factor of two of the “recommended” MCNPX-BERTINI results.

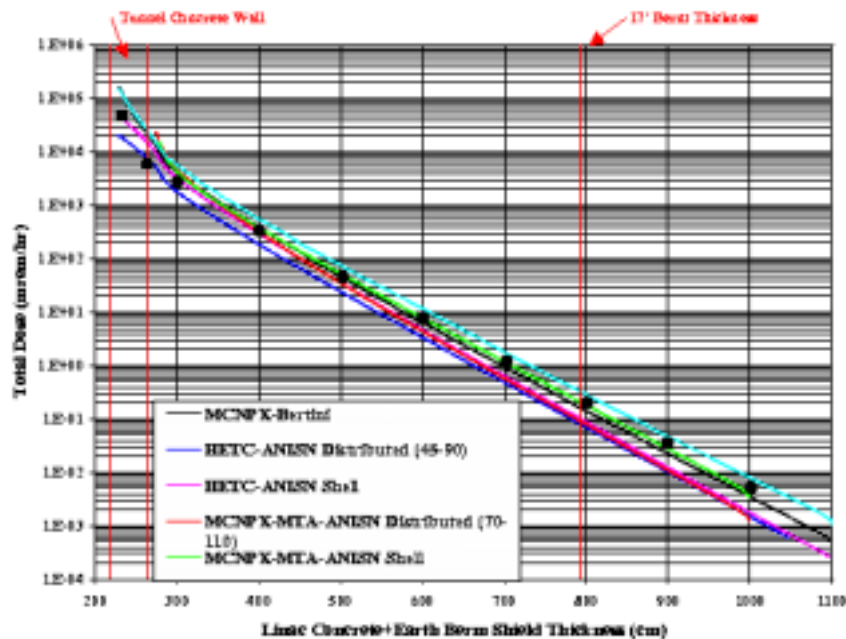


**Figure 10.1.** Dose attenuation in the ORNL SNS Linac earth berm [15] as calculated by ORNL group (lines) and with MARS14 (symbols).

Another recent benchmark [16] was performed for a 2-m long cylinder—representative of the forward shielding of the CMS detector at LHC—for a 10 GeV/c pencil proton beam hitting it. The absorber consisted radially of iron ( $0 < r < 40$  cm), concrete ( $40 < r < 100$  cm), borated polyethylene ( $100 < r < 110$  cm) and air at  $110 < r < 120$  cm. Fig. 10.2 shows almost perfect agreement of MARS14 and FLUKA [12] for energy-integrated neutron fluxes. Both codes reproduce similarly the physics of interactions in different materials in the energy range spanning tens of GeV down to a fraction of an electronvolt.

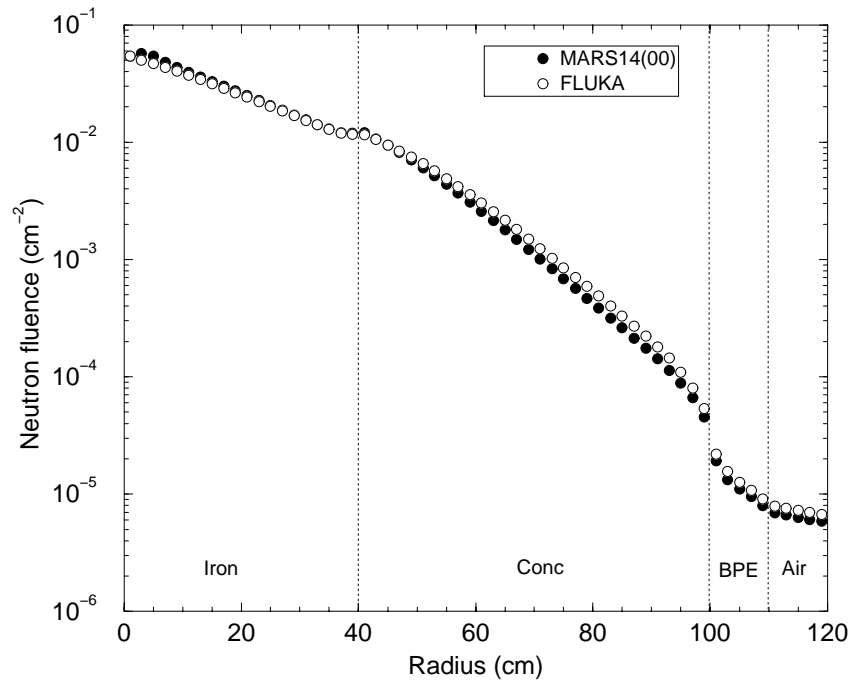


**Figure 10.2.** Total neutron fluence at  $50 < z < 100$  cm in a 2-m composite cylinder irradiated by a 10 GeV/c pencil proton beam as calculated by MARS14 and FLUKA.

#### 10.4.4. Tunnel shielding

The following approach to shielding design is used in this study. Both normal operation and accidental beam losses are considered at injection through the top energy. Realistic beam loss distributions of Chapter 9 are used as a source term for normal operation wherever they are available. A simplest operational scenario with a 1 W/m beam loss rate is assumed otherwise. Local shielding is provided around the components in all cases where hands-on maintenance limits on the component outer surface or radiation load to ground water around the tunnel walls in this region are exceeded. This equalizes (to some extent) the source term for the dirt shielding calculation around the entire machine. For accidental beam loss, both the worst case catastrophic *incredible* and *credible* accidents are considered: a point-like loss of  $1.62 \times 10^{18}$  protons for an hour (*incredible* accident) and 0.1% of that (*credible* accident). The maximum thickness from all cases considered is put into the design as the tunnel shielding in that part of the machine.

Dose on the outer shielding surface depends on the beam energy in a complex way. Assuming a quasi-local beam loss in the magnet, dose equivalent was calculated with MARS14 as a function of dirt thickness ( $\rho = 2.24 \text{ g/cm}^3$ ) outside the tunnel walls. Fig. 10.3 shows this dependence for a 400 MeV beam (injection), for two intermediate energies of 3 and 8 GeV, and for the top beam energy. Dose at high energies scales as  $E^\alpha$ , where  $\alpha$  is about 0.8, while  $\alpha \geq 1$  at proton energies below about 1 GeV.

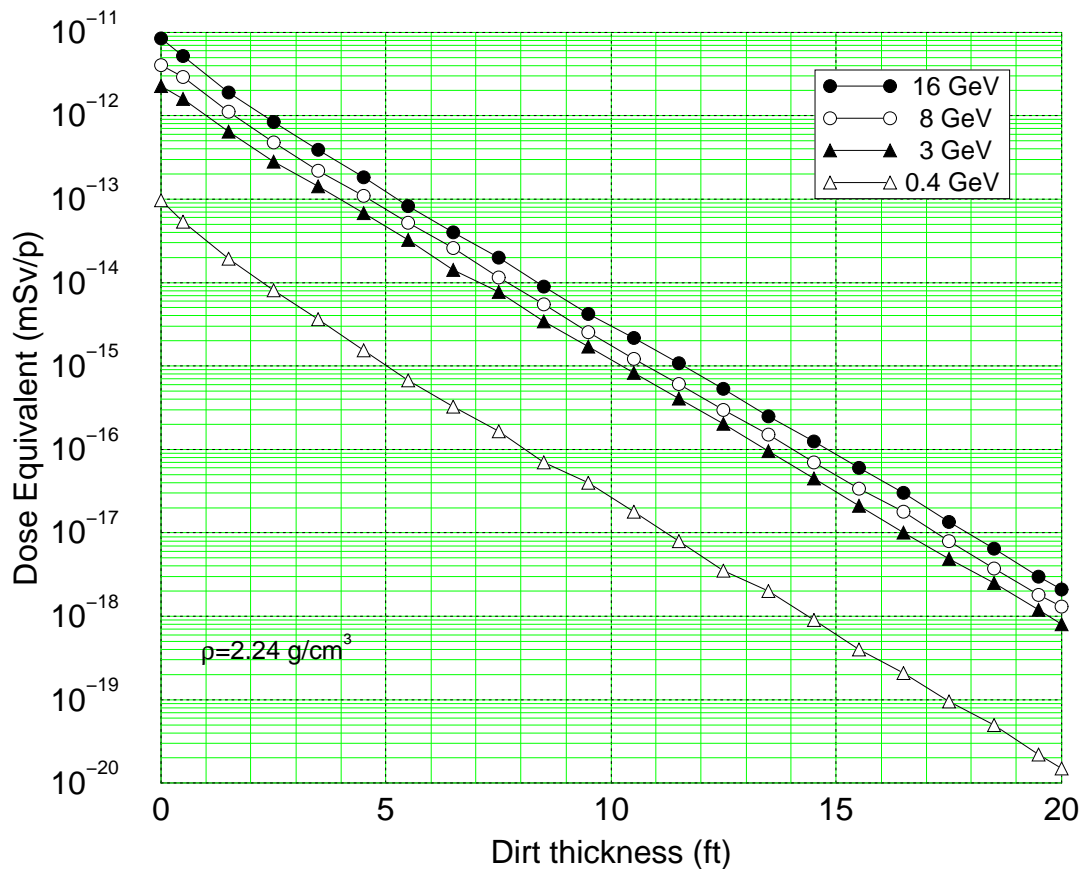


**Figure 10.3.** Prompt dose equivalent vs dirt thickness around the tunnel at a point-like loss of proton beams of different energies.

For the 16 GeV 15 Hz Proton Driver with  $3 \times 10^{13}$  circulating protons, the dose which corresponds to the 1 mrem limit for the worse case point-like loss of  $1.62 \times 10^{18}$  protons for an hour is  $D_0 = 6.18 \times 10^{-24}$  Sv per proton (1 Sv = 100 Rem), requiring about 28 feet of the dirt shielding around the tunnel. With the accidental beam loss of 0.1% of the above—that can be defined as a *credible* accident for this machine—the shield thickness at 16 GeV is reduced to 18.5 feet. In normal operation, the shielding required is noticeably thinner. With the uniformly distributed beam loss rate of 1 W/m in the magnets—which is equivalent to about  $3.9 \times 10^8$  p/m/s lost at 16 GeV—the dirt shielding thickness needed to reduce the dose to 0.05 mrem/hr is  $\sim 14$  feet. This thickness can be even smaller if one takes into account the lower average beam loss rates in some regions as calculated in Chapter 9.

## 10.5. Beam Transport Line Shielding

As Chapter 18 suggests, from the standpoint of machine reliability, a *credible* accident is defined for beam transport lines as a point-like loss of the full beam continuing for one sec-

ond during a given one hour period of operations, resulting in  $N_A$  (p/sec) lost in a beam-line element. Lateral shielding of thickness  $t_A$  must provide attenuation of the dose at non-controlled areas on accessible outside surfaces of the shield to 1 mrem/hr.

For normal operation of the beam transport lines, we assume at this stage 0.1% loss over the line length, resulting in a uniform beam loss along a beam line at a  $N_O$  (p/m/sec) rate. Lateral shielding of thickness  $t_O$  must provide attenuation of the dose at non-controlled areas on accessible outside surfaces of the shield to 0.05 mrem/hr. Material of the lateral shielding outside the tunnel walls is assumed to be Fermilab wet dirt of density  $\rho = 2.24 \text{ g/cm}^3$ .

### 10.5.1. Injection

Accidental 0.4-GeV beam loss of  $N_A = 4.95 \times 10^{14}$  (p/sec) requires  $t_A = 10.5$  feet of dirt. Operational 0.4-GeV beam loss of  $N_O = 1.65 \times 10^9$  (p/m/sec) = 0.106 W/m along a 300-m long injection beam line requires  $t_O = 9.5$  feet of dirt. Assuming a safety factor of 3, the thickness of dirt shielding above the 0.4-GeV injection beam line is 12 feet. Phase II (4 MW, 1 GeV) will require about 15.25 feet of dirt.

### 10.5.2. Extraction

Accidental 16-GeV beam loss of  $N_A = 4.5 \times 10^{14}$  (p/sec) requires  $t_A = 17$  feet of dirt. Operational 16-GeV beam loss of  $N_O = 4.5 \times 10^8$  (p/m/sec) = 1.152 W/m along a 1000-m long extraction beam line requires  $t_O = 14.5$  feet of dirt. Assuming a safety factor of 3, the thickness of dirt shielding above the 16-GeV extraction beam line is 18.5 feet. Phase II (4 MW) will require about 20 feet of dirt.

## 10.6. P10, P30 and P50 Arc Shielding

As described in Section 10.4.2, MARS14 simulations in the arcs are done first for longitudinally uniform 16-GeV beam loss and then for realistic beam loss distributions from Chapter 9. The full arc lattice in a rectangular tunnel embedded into wet Fermilab dirt is implemented into the MARS calculation model. The tunnel width is 16 feet, its height is 9 feet, the concrete walls are 15-inch thick, ceiling and floor are 30-inch thick. The lattice elements as modeled in MARS are described in Chapter 9. Fig. 10.4 shows a plan view of the arc tunnel with magnets as implemented into the model, while cross-sectional views are shown in Fig. 10.5. Cable trays are positioned at the ceiling in the left and right corners of the cross-sections shown.

### 10.6.1. Prompt radiation

Even with the beam lost uniformly along the arc lattice, there are pronounced peaks of radiation field around the long bare beam pipes. These could dominate the radiation environment near the beam line. Fig. 10.6 shows hadron flux distributions across the lattice elements, tunnel, its walls and first layers of the surrounding dirt. The flux and, as a result, all other radiation values are about a factor of ten higher on the long bare beam pipe compared to that on the magnet outer surfaces. At large distances from the lattice elements, at

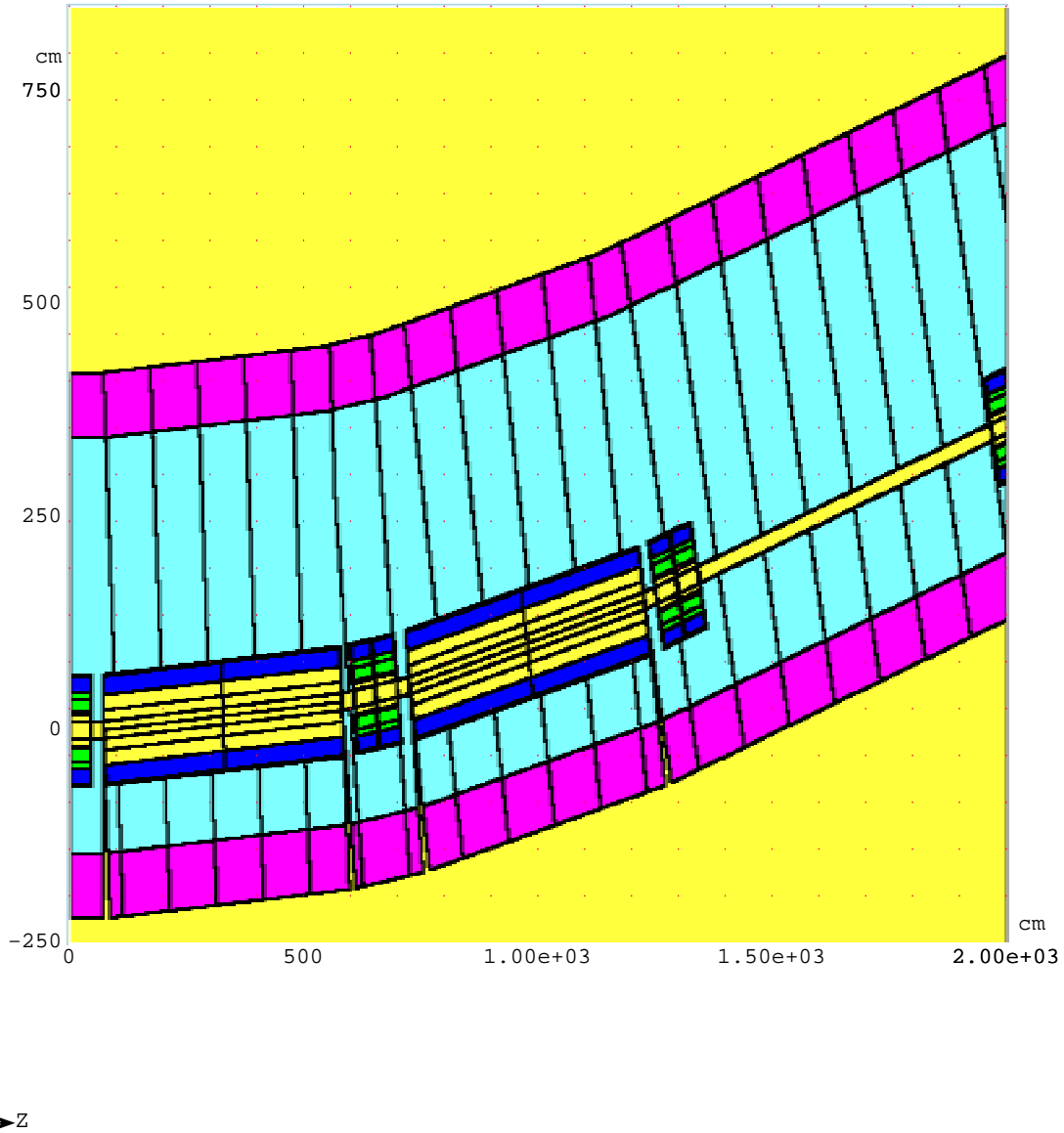


**Figure 10.4.** Plan view of the modeled arc.

tunnel walls, ceiling and floor, and in the surrounding dirt, the radiation levels are much more uniform longitudinally and transversely. In the model considered, the hadron flux immediately outside the tunnel walls near the peaks in the magnets is below the limit of  $\Phi_h^0(E > 20 \text{ MeV}) = 3850 \text{ cm}^{-2}\text{s}^{-1}$ . The flux outside of the inward tunnel wall and under the floor near the long bare beam pipe peaks is above the limit by a factor of 3 to 5, while it is right on the limit above the ceiling and outside the outward wall. This implies that either the beam loss rate on the long bare beam pipes should be kept below 0.2-0.3 W/m or these regions require local shielding.

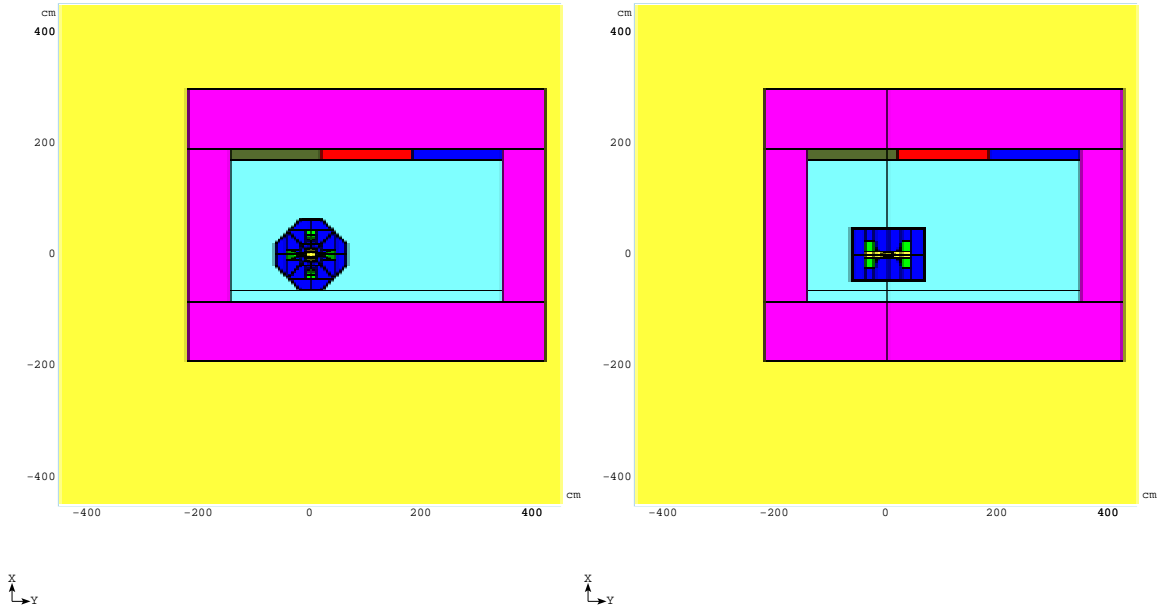


**Figure 10.5.** Cross-sectional views of the modeled arc at quadrupole (left) and dipole (right) locations.

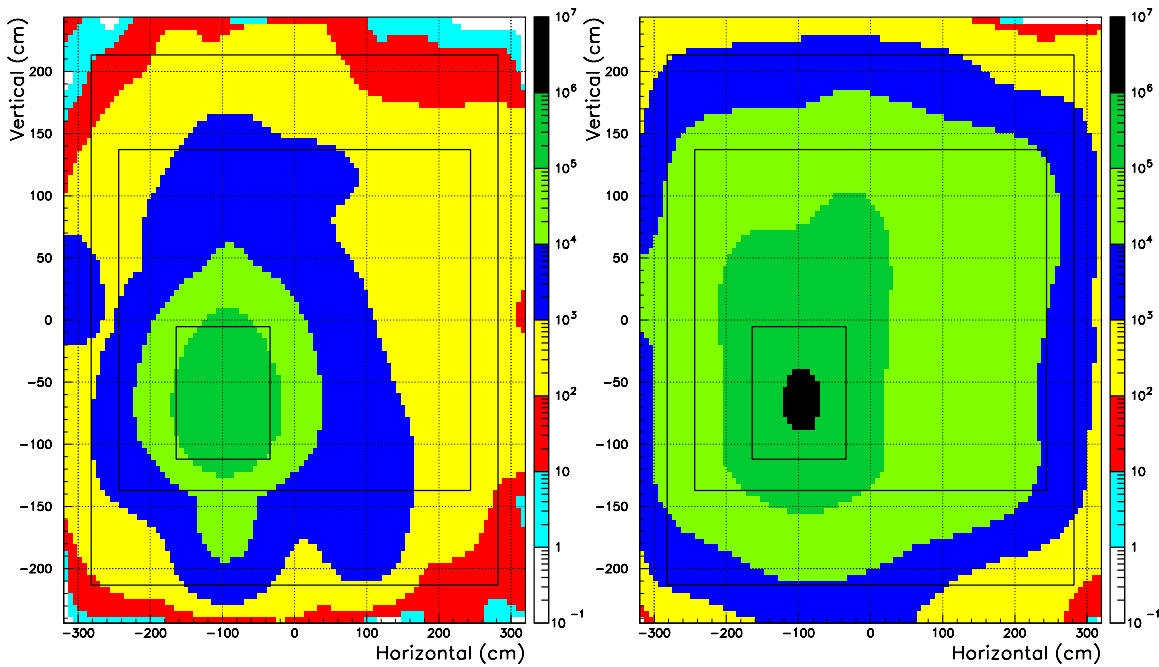


**Figure 10.6.** Hadron ( $E > 20$  MeV) isofluxes ( $\text{cm}^{-2}\text{s}^{-1}$  at 1 W/m) in the arc tunnel cross-section at peak at a dipole magnet (left) and long drift (right).

Despite variation in realistic beam loss distribution along the lattice and remembering the fact that the shield thickness is driven by accidental beam loss which can take place in an arbitrary lattice location, a uniform shielding design along the arcs is suggested. With the worst case point-like accidental loss of 0.1% of the 1-hour beam intensity at 16 GeV—a *credible* accident for the arcs and long straight sections—the shield thickness required is 18.5 feet of Fermilab wet dirt. At normal operation, it is about 14 feet. Assuming a safety factor of 3, the thickness of dirt shielding above the arcs is 20 feet. Phase II (4 MW) will require about 21.5 feet of dirt.

Fig. 10.7 shows annual dose distributions in the same arc cross-sections at a dipole magnet and long drift peaks. The maximum dose accumulated in the coils is about 2 Mrad/yr at 1 W/m beam loss rate which is acceptable with use of appropriate materials for insulation. Care should be taken of cable insulation, possible oil and electronics in the tunnel. The maximum annual dose at cable locations at the ceiling is about 0.1-0.2 Mrad/yr above the magnet hot spots, and is about 0.3-0.5 Mrad/yr above the 6-m long bare beam pipes at 1 W/m beam loss rate.

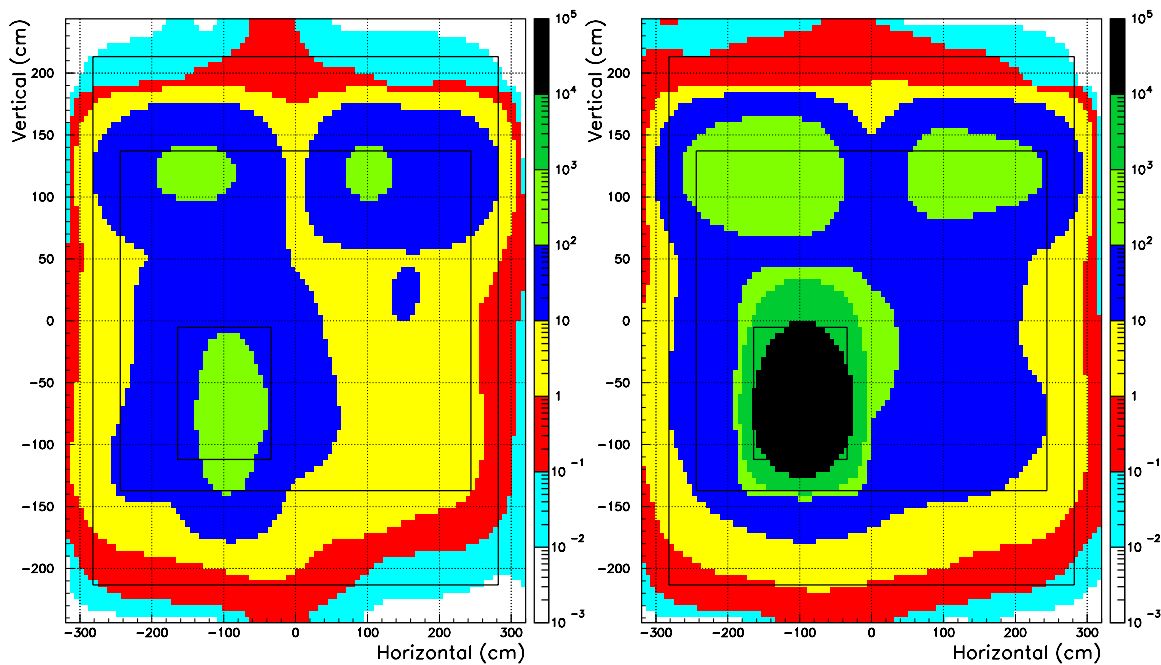


**Figure 10.7.** Isodose distributions (krad/yr at 1 W/m) in the arc tunnel cross-section at peak at a dipole magnet (left) and long drift (right).

### 10.6.2. Residual radiation

Calculated peak residual dose rates on contact are shown in Fig. 10.8 for 30 days of irradiation at 1 W/m uniform beam loss rate and 1 day of cooling. Remember that these conditions give results very close to 100 day irradiation and 4 hours cooling for the dose at 30 cm radial distance from the component surface. The dose near the bare beam pipes exceeds the design goal for hot regions of 100 mrem/hr, being noticeably lower near the magnets due to signifi-

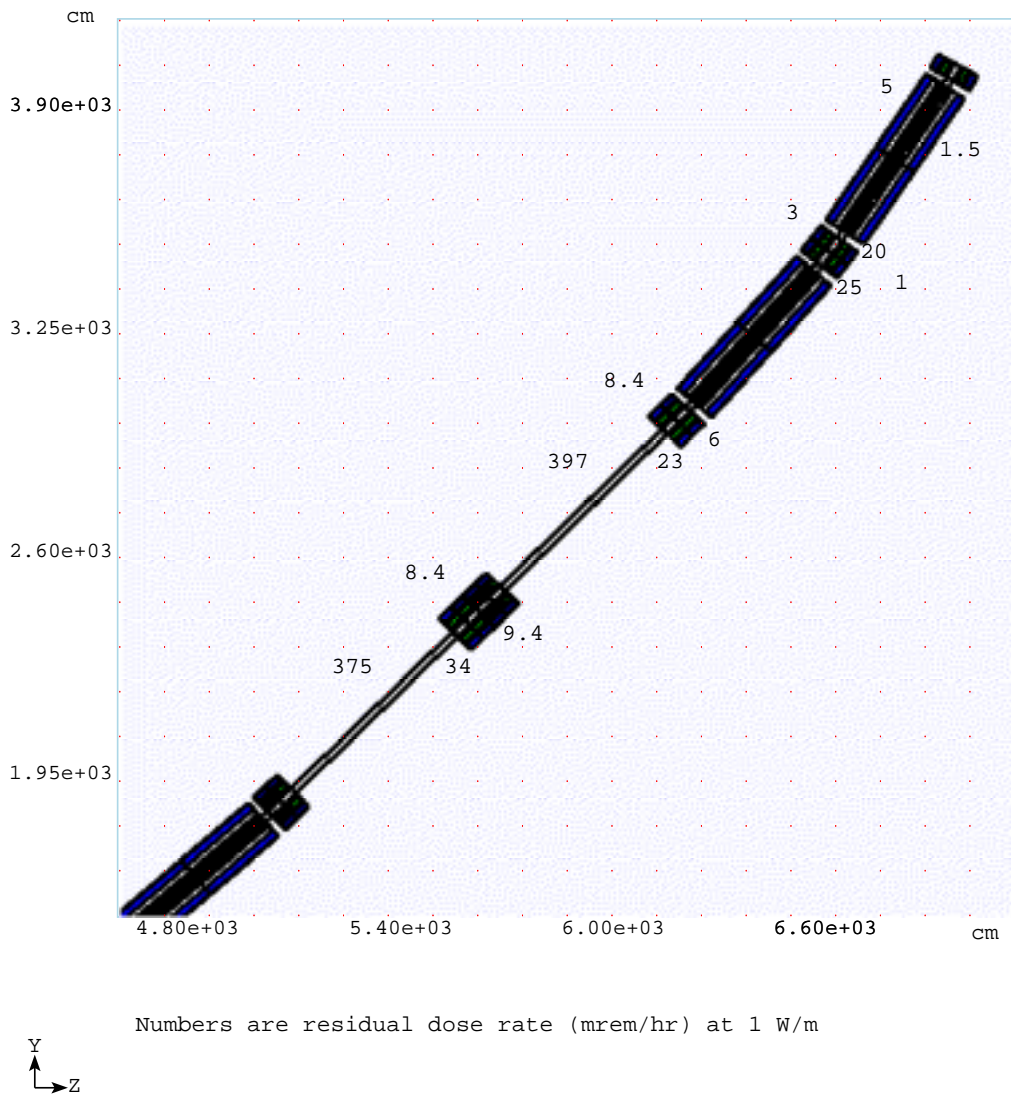


**Figure 10.8.** Peak residual dose rates (mrem/hr) on the outer surface of the arc elements at 1 W/m uniform beam loss rate at 16 GeV.

cant absorption of soft photons in the dipole and quadrupole materials. One sees that hands-on maintenance is a serious issue with about 3 W/m as a tolerable maximum beam loss rate in the lattice elements, except for the long bare beam pipes where one should decrease the loss rate to 0.25 W/m to reduce the dose to 100 mrem/hr. One needs further reduction to bring the dose down to a good practice value of about 10-20 mrem/hr. Alternatively, one can think of providing simple shielding around the bare beam pipes. For ground-water activation immediately outside the tunnel walls, the peak values are below the limit around the magnets, but are 2 to 3 times above the limit at 1 W/m beam loss rate on bare beam pipes.

At 16 GeV the determining factor is hands-on maintenance, with about 3 W/m as a tolerable maximum beam loss rate in the lattice elements, except for the open long beam pipes. There one should reduce the loss rate to 0.25 W/m to reduce the dose to 100 mrem/hr. One needs further reduction to bring the dose down to a good practice value of about 10-20 mrem/hr. Alternatively, one can think of providing simple shielding around the bare beam pipes.

## 10.7. P20 Long Straight Shielding

The P20 long straight section, with the injection system and with the collimation system intercepting about 99% of beam loss, is the hottest region in the machine. The beam loss distribution of Chapter 9 is used as a source term in the MARS14 simulations in this region. It is assumed that 10% of the intensity is intercepted at injection, and 1% at the top energy. The region considered includes all the components of the P20 long straight section (see Fig. 9.1) as shown in Fig. 10.9. The secondary copper collimators are 0.5-m long and  $44 \times 44 \text{ cm}^2$  transversely. They are the hottest spots, with beam loss rates of several kW/m.

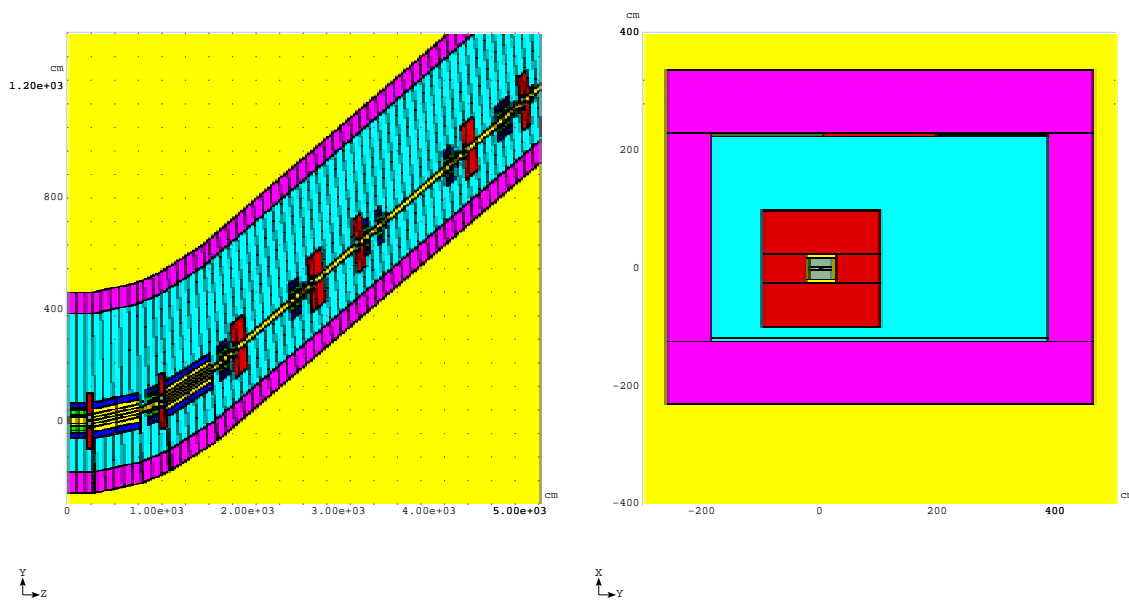


**Figure 10.9.** Longitudinal view of the collimation region (left) and cross-sectional view at the C1 collimator (right) with the proposed shielding as implemented into the MARS14 calculation model.

### 10.7.1. Prompt radiation

To meet the regulatory requirements for hands-on maintenance and ground-water activation, massive shielding is required in the P20 region. Calculations show that the optimal configuration would include local shielding around collimators along with extended shielding over the entire region. Local steel shielding is 2.5 m long and extends to  $|x, y|=115 \text{ cm}$  transversely around all secondary collimators, dipoles and quadrupoles downstream. To ac-

comodate this shielding, the P20 tunnel interior is enlarged by 90 cm horizontally and vertically. Hadron flux distributions at the secondary collimator C2 and supplementary collimator SC3 (see Fig. 9.1) are shown in Fig. 10.10 and Fig. 10.11 (left). With such a shield, radiation levels outside the tunnel wall are very close to those in the arcs. Therefore, the same external shielding design both for normal operation and beam accident is applied. With a safety factor of 3, the thickness of dirt shielding above the P20 long straight section is 20 feet, increased to about 21.5 feet at Phase II (4 MW).

Fig. 10.11 (right) shows annual dose distribution in the P20 tunnel cross-section at the C2 collimator. The maximum dose accumulated in the collimator cores is several hundred Mrad/yr. The maximum annual dose at cable locations at the ceiling is about 50 krad/yr.

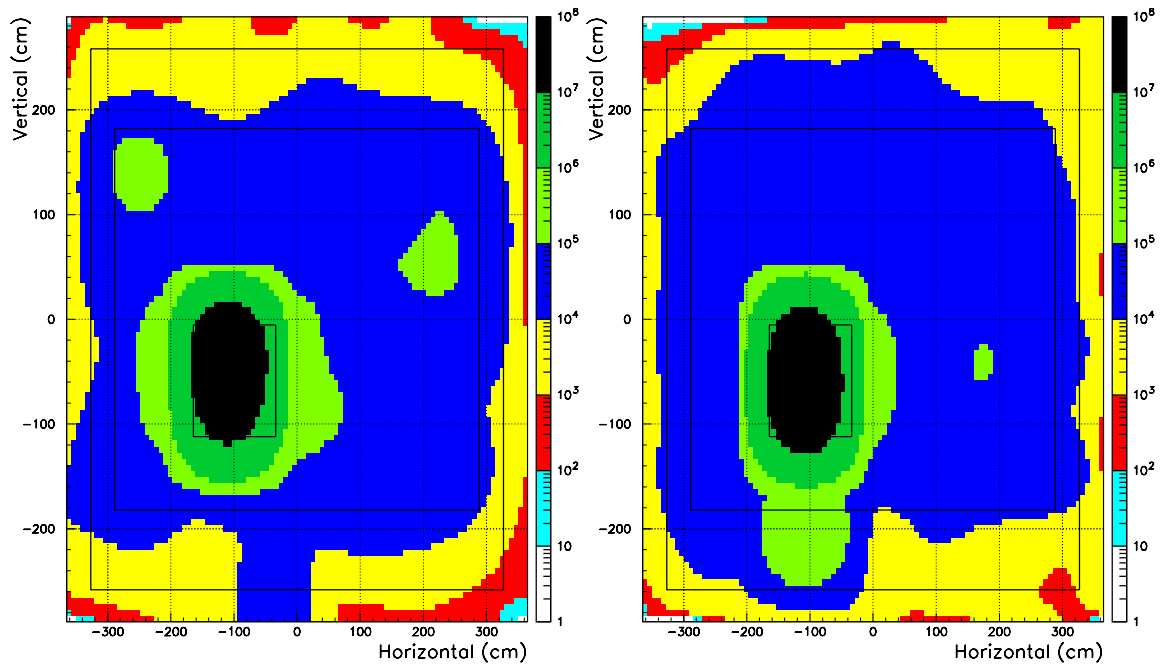


**Figure 10.10.** Hadron ( $E > 20$  MeV) isoflux ( $\text{cm}^{-2}\text{s}^{-1}$ ) in the P20 tunnel cross-section at the collimators C2 (left) and SC3 (right).

### 10.7.2. Residual radiation

As shown in Fig. 10.10, the hadron flux immediately outside the tunnel walls averaged over each side exceeds by about a factor of three the limit of  $\Phi_h^0(E > 20 \text{ MeV}) = 3850 \text{ cm}^{-2}\text{s}^{-1}$ , that corresponds to the ground water activation limit  $C_{tot} = 1$  in (10.2). This implies that the P20 tunnel wall thickness should be increased by about one foot, which may also be needed because of the large tunnel cross-section.

Residual dose rates on the outer surface of the proposed shielding do not exceed 20 mrem/hr after a 30 day irradiation and 1 day cooling. Taking into account all the current uncertainties, one can use the proposed configuration as a baseline for further studies.

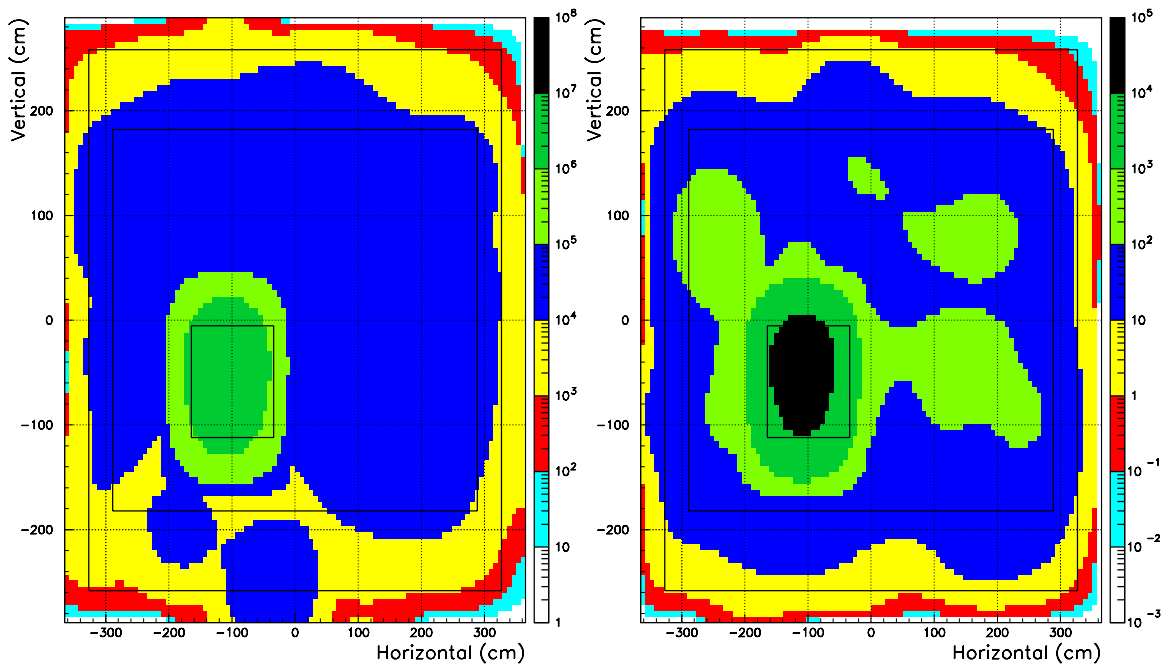


**Figure 10.11.** Hadron ( $E > 20$  MeV) isoflux ( $\text{cm}^{-2}\text{s}^{-1}$ ) in the P20 tunnel cross-section two meters downstream of the collimator C3 (left) and isodose distribution (krad/yr) at the secondary collimator C2 (right).

It is interesting to note that the dose peaks are located about 2 m downstream of the collimators and the corresponding peaks in the beam loss distribution. These are a source of secondary particles irradiating the downstream quadrupoles. To provide adequate protection against low-energy neutrons at the hot spots, homogeneous liners (0.3 m thick concrete or polyethylene) inside and outside the steel shielding might be needed.

The ultimate shielding design will include material cost/volume minimization as well as civil construction, cooling and remote control. There are many engineering design issues in this region. The local shielding weight is about 12 ton/m. It occupies significant cross-sectional area and makes access to the region components a non-trivial task. Radiation levels inside it are extremely high preventing hands-on maintenance. Therefore the design should include a remotely operated crane to lift out the shielding and parts of the beam-line. The beam-line elements should be designed for fast remote maintenance. Remote operations are required for fine tuning of the collimator jaws. Another problem is the heat buildup in the collimation system. The power intercepted by the collimators C1 and C2 is equal to about 3 and 4 kW, respectively. It is dissipated in the collimators themselves and along 2-3 meters in the downstream beam-line. A cooling system should be able to remove this power. Radiation damage to the cables, cooling water pipes, beam diagnostics elements and other sensitive components is a serious issue in this region and will be considered for the entire machine in the near future.

## 10.8. P40 and P60 Long Straight Shielding

Extraction from the Proton Driver will be one-turn fast extraction. In order to reduce the extraction loss in Stage 1, there will be a 7-bucket notch in a train of 126 bunches. Therefore, there will be little loss at the extraction septum. In Stage 2, this notch is not needed due to a large bunch spacing (132 ns). When the machine is well tuned, the extraction loss can be as low as the order of  $10^{-4}$ , which has been achieved at the ISIS. As for the RF cavities with large apertures, our calculations show no noticeable beam loss in those regions.

The above implies that no local shielding is needed in the P40 and P60 long straight sections. At this stage, shielding design and radiation requirements in these regions are assumed the same as in the arcs.

## References

- [1] J. O. Johnson, "Radiation Transport Analyses for the U. S. Spallation Neutron Source (SNS)", in *Proc. of the Monte Carlo 2000 International Conference*, Lisbon, Portugal, October 23-26 (2000).
- [2] O. E. Krivosheev and N. V. Mokhov, "Tolerable Beam Loss at High-Intensity Proton Machines", in *Proc. of the 7th ICFA Mini-Workshop on High-Intensity, High-Brightness Hadron Beams "Beam Halo and Scraping"*, Lake Como, Wisconsin, September 13-15, 1999, Fermilab-Conf-00/185, Fermilab-Conf-00/192 (2000).
- [3] A. I. Drozhdin, O. E. Krivosheev and N. V. Mokhov, "Beam Loss, Collimation and Shielding at the Fermilab Proton Driver", Fermilab-FN-693 (2000).
- [4] "Fermilab Radiological Control Manual", Article 236, <http://www-esh.fnal.gov/FRCM/>.
- [5] J. D. Cossairt, Private communication (2000).
- [6] N. Grossman et al., "Refinement of Groundwater Protection for the NuMI Project", Fermilab-TM-2103 (2000).
- [7] J. D. Cossairt, A. J. Elwyn, P. Kesich, A. Malensek, N. V. Mokhov, and A. Wehmann, "The Concentration Model Revisited", Fermilab-EP-Note-17 (1999).
- [8] J. O. Johnson, Private communication, ORNL (2000).

- [9] N. V. Mokhov, “The MARS Code System User’s Guide”, Fermilab-FN-628 (1995); N. V. Mokhov, S. I. Striganov, A. Van Ginneken, S. G. Mashnik, A. J. Sierk, and J. Ranft, “MARS Code Developments”, Fermilab-Conf-98/379 (1998); N. V. Mokhov, “MARS Code Developments, Benchmarking and Applications”, Fermilab-Conf-00/066 (2000). N. V. Mokhov and O. E. Krivosheev, “MARS Code Status”, Fermilab-Conf-00/181 (2000). <http://www-ap.fnal.gov/MARS/>.
- [10] D. N. Mokhov, O. E. Krivosheev, E. McCrory et al, “MAD parsing and conversion code”, Fermilab-TM-2115 (2000).
- [11] I. S. Baishev, A. I. Drozhdin and N. V. Mokhov, “STRUCT Program User’s Reference Manual”, SSCL-MAN-0034 (1994); <http://www-ap.fnal.gov/~drozhdin/STRUCT/STR2.html>.
- [12] P. A. Aarnio *et al*, CERN TIS-RP/168 (1986) and CERN TIS-RP/190 (1987). A. Fassøet *al*, *Proc. IV Int. Conf. on Calorimetry in High Energy Physics*, La Biodola, Sept 20-25, 1993, Ed. A. Menzione and A. Scribano, World Scientific, p. 493 (1993). P. Aarnio and M. Huhtinen, *Proc. MC93, Int. Conf. on Monte Carlo Simulation in High Energy and Nuclear Physics*, p 1, ed. P. Dragowitsch, S. Linn and M. Burbank, World Scientific (1994). A. Fassøat *al*, *Proc. Specialists’ Meeting on Shielding Aspects of Accelerators, Targets and Irradiation Facilities*, Arlington, Texas, April 28-29, 1994. NEA/OECD doc., p. 287 (1995).
- [13] A. Fassø, A. Ferrari, J. Ranft, P.R. Sala, “New developments in FLUKA modelling hadronic and EM interactions”, *Proc. 3rd Workshop on Simulating Accelerator Radiation Environments*, KEK, Tsukuba, Japan, 7-9 May 1997, Ed. H. Hirayama, KEK Proceedings 97-5, p. 32-43. A. Ferrari, and P.R. Sala, “The Physics of High Energy Reactions”, *Proc. the Workshop on Nuclear Reaction Data and Nuclear Reactors Physics, Design and Safety*, International Centre for Theoretical Physics, Miramare-Trieste, Italy, 15 April-17 May 1996, edited by A. Gandini and G. Reffo, World Scientific, p. 424 (1998).
- [14] <http://mcnpx.lanl.gov>.
- [15] J. O. Johnson et al., “The Independent Verification and Validation of the ORNL SNS Linac Earth Berm Shielding Analysis”, ORNL-SNS/TSR-177 (2000).
- [16] M. Huhtinen and N. V. Mokhov, “A Cross-comparison of MARS and FLUKA Simulation Codes”, Fermilab-FN-697 (2000).